nature sensors

Article

https://doi.org/10.1038/s44460-026-00037-z

Tunable and highly sensitive functionalized carbon-nanotube-based integrated systems for chemical gas sensing

Received: 22 May 2025

Accepted: 28 January 2026

Published online: 25 February 2026

Check for updates

Jaekang Song[1,6], Dong-Ha Kim[2,3,6], Jan Tiepelt[1], Young-Moo Jo[2,5], Graham McGrath[4], Michael Song[4], Tianyang Chen[2], Jiande Wang[2], Alicia Coto[4], Sundar Palani[4], Dooyong Koh[1], Samuel Fuller[4], Max Shulaker[1,4] ✉, Mircea Dincă[2] ✉ & Marc Baldo[1] ✉

Chemical gas sensing is essential for healthcare, environmental monitoring and industrial safety, yet current sensors lack sensitivity, selectivity and scalability. Carbon nanotube field-effect transistors (CNFETs) offer high surface area and low-power operation, but they traditionally provide limited chemical discrimination. Here we report an integrated sensing platform that combines CNFETs with conductive metal–organic frameworks and catalytic metal nanoparticles to achieve tunable selectivity and enhanced sensitivity. The hybrid architecture boosts response by up to two orders of magnitude and enables on-chip pattern generation for robust gas classification. As proof of concept, we apply the platform to the classification of clinically relevant bacteria and yeast species by analysing the volatile organic compounds emitted from cultures grown on agar plates with 95% accuracy, using a portable measurement set-up. By integrating functionalized CNFETs into a commercial foundry-derived system, this work introduces a rapid, cost-effective and scalable gas sensing approach for real-world biomedical and industrial sensing applications.

The microelectronics revolution has been driven by commodity manufacturing of complex systems with unprecedented capability. One domain, however, has remained relatively untouched—chemical gas sensing. In response, research has focused on novel electronic materials[1], new device structures for better transduction of chemical and biological information[2], and new integrated systems[3,4] that mimic the multichannel olfactory systems of living organisms.

Among electronic materials used for sensing, carbon nanotubes (CNTs) are notable for their high surface-to-volume ratio, accessible surface chemistry[5], low power consumption[6] and room-temperature operation for compatibility with biological and medical applications[7]. To overcome the inherent selectivity limits of pristine CNTs, extensive efforts have been dedicated to tuning the surface chemistry of CNTs through catalyst decoration[8], polymer wrapping[9], anchoring of acceptors[10] or constructing heterogeneous structures[11]. Nevertheless, achieving high sensitivity and tunable selectivity, as well as understanding the underlying sensing mechanisms of CNT-based sensors, remains challenging.

In this work, we present a sensor array utilizing commercial foundry-derived CNT-based integrated sensors containing 2,048

[1]Research Laboratory of Electronics, Massachusetts Institute of Technology, Cambridge, MA, USA. [2]Department of Chemistry, Massachusetts Institute of Technology, Cambridge, MA, USA. [3]Department of Materials Science and Chemical Engineering, Hanyang University, Ansan, Republic of Korea. [4]Analog Devices Incorporated, Wilmington, MA, USA. [5]Present address: School of Materials Science and Engineering, Kyungpook National University, Daegu, Republic of Korea. [6]These authors contributed equally: Jaekang Song, Dong-Ha Kim. ✉e-mail: Max.Shulaker@analog.com; mdinca@mit.edu; baldo@mit.edu

https://doi.org/10.1038/s44460-026-00037-z

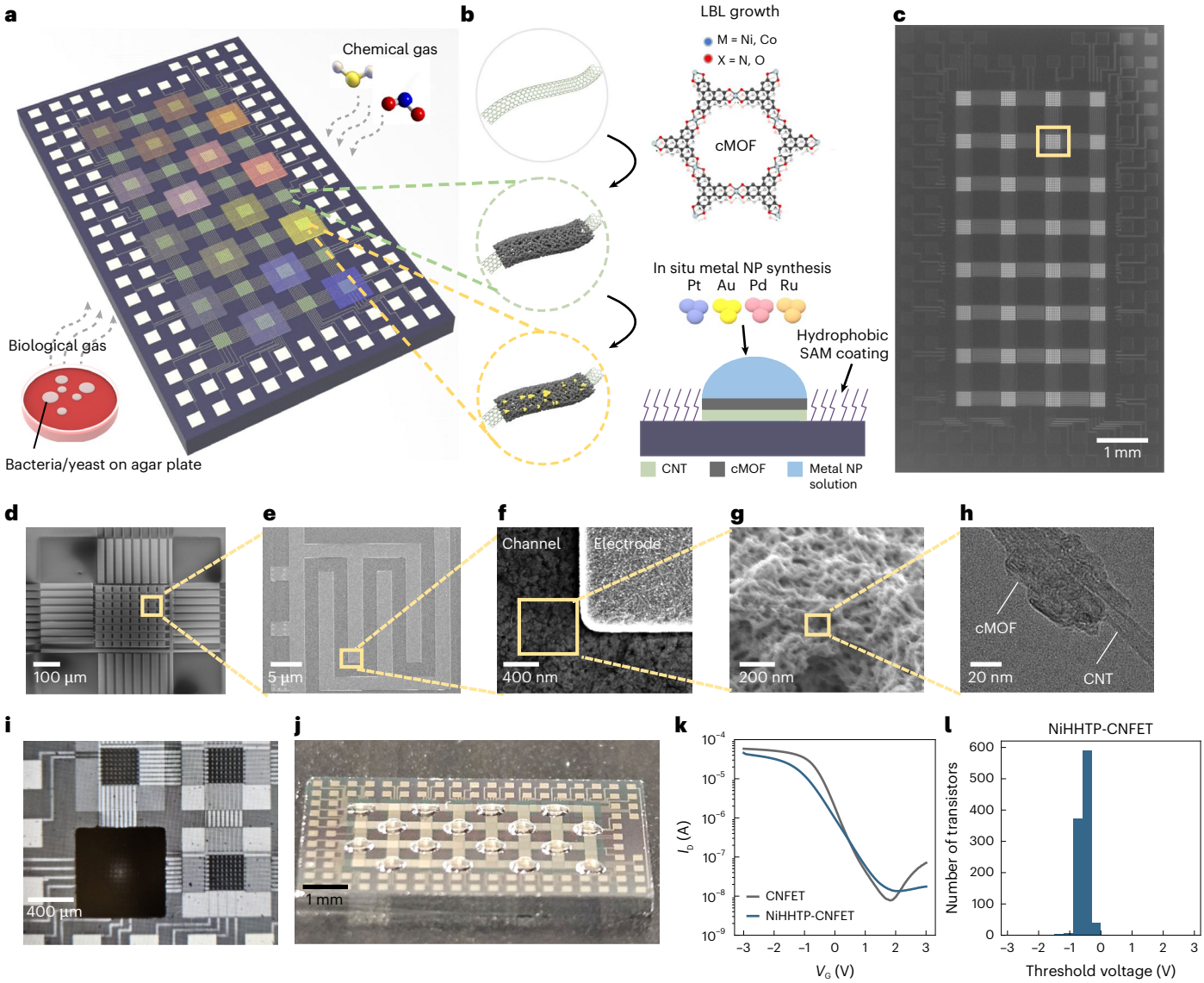

Fig. 1 | Chip functionalization. a, Chip schematics. The CNFET chip has 32 subarrays, each containing 64 CNFETs. cMOFs are grown on all 32 subarrays, and 16 selected subarrays are further functionalized with 4 distinct metal nanoparticles at 4 different concentrations. **b**, Device functionalization flow. Insets: CNT (top), cMOF-functionalized CNT (middle) and cMOF-functionalized CNT with metal nanoparticles (NP) (bottom). The first functionalization is LBL growth of cMOF, and the second is in situ synthesis of metal nanoparticles after forming microfluidic boundary. **c**, An OM image of a CNFET chip. A subarray is shown in a yellow rectangle. **d**–**g**, A SEM image of a subarray containing 64 CNFETs (**d**), a CNFET with interdigitated electrodes (**e**), the interface between the channel and electrode after cMOF growth (**f**) and a CNT channel after cMOF growth (**g**). **h**, A TEM image of cMOF-functionalized CNT. **i**, An OM image of a subarray fully filled with metal nanoparticle solution without overflow. **j**, An image of a chip where metal nanoparticle solutions are drop cast onto 16 selected subarrays. **k**, Average transfer characteristics of all NiHHTP-CNFETs on a chip, where I_D (A) is the drain current. **l**, Histogram of threshold voltage after cMOF growth.

CNT field effect transistors (CNFETs), functionalized with electrically conductive metal–organic frameworks (cMOFs) and catalytic metal nanoparticles. The cMOFs are highly porous and easily tunable electronic materials[12]. We show that cMOF functionalization enhances the sensor sensitivity by up to two orders of magnitude and modulates the selectivity to the target gases. To create sensors with different sensitivities for on-chip pattern generation, we define subarray areas by forming microfluidic boundaries through a self-assembled monolayer (SAM) process and perform in situ synthesis of Pt, Au, Pd and Ru metal nanoparticles on the surface and within the pores of the cMOF. The performance and operating mechanism of the chip is characterized using redundancy within the 2,048 functionalized CNFETs to generate statistically significant results for an array of gases. Then, highlighting the potential of the integrated circuits for medical applications, we demonstrate a representative application: classifying *Escherichia coli* (EC), *Pseudomonas aeruginosa* (PSA) and *Candida albicans* (CA) based on the mixture of gases released from the microorganisms in culture. Our successful demonstration promises convenient, safe, rapid bacterial and yeast differentiation in clinical settings.

Functionalization of CNFET chips

CNFET chips are fabricated on a conventional 200-mm silicon substrate[13] and subsequently diced into 6 × 10 mm^2 dies, each corresponding to a single sensing unit (Methods). Each sensing chip comprises 2,048 global back-gated CNFETs, divided into 32 subarrays, with each subarray containing 64 CNFETs (Fig. 1a). We enhance the response of the chips to target gases and differentiate the sensors using a scalable two-step functionalization process (Fig. 1b).

https://doi.org/10.1038/s44460-026-00037-z

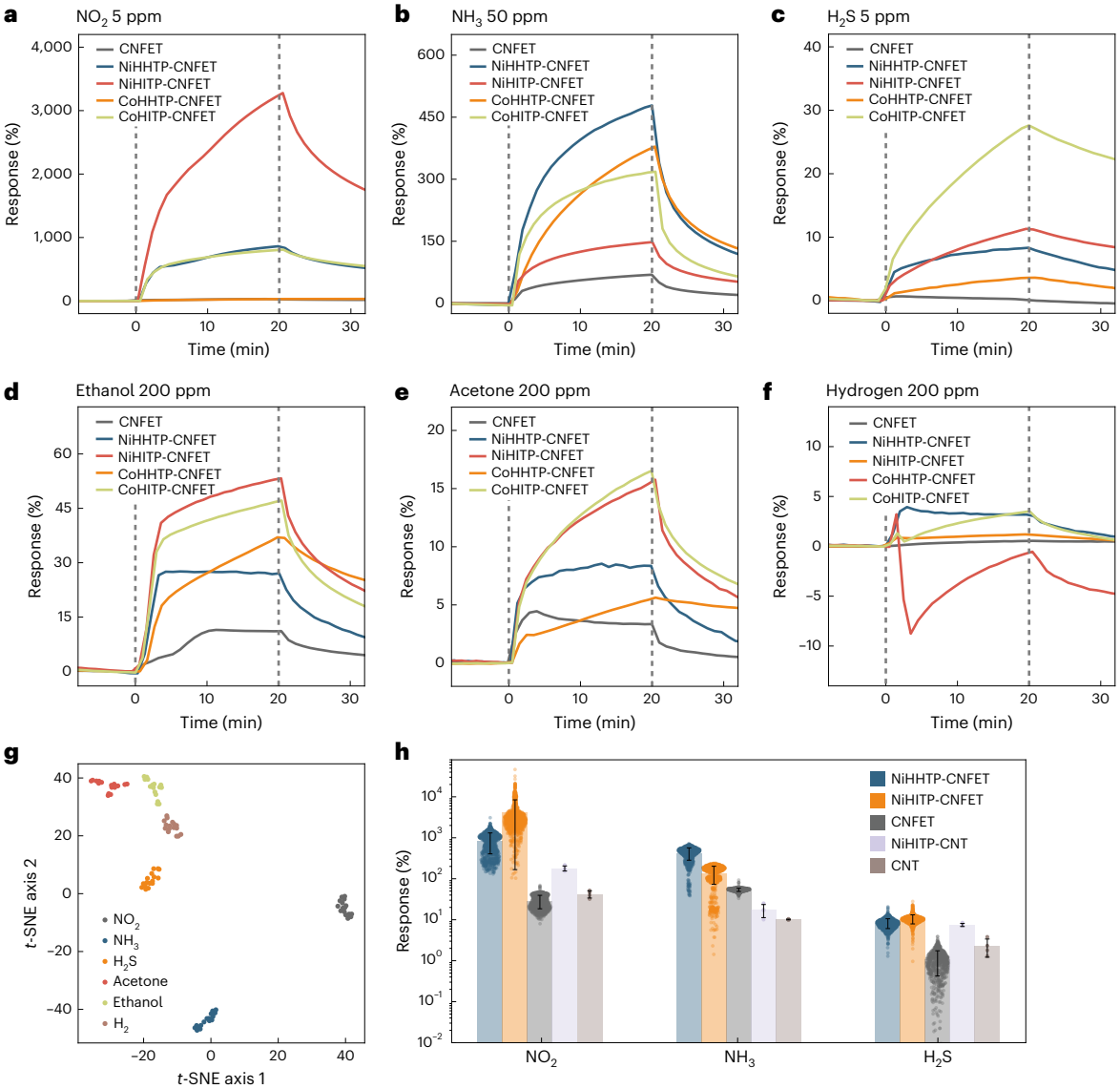

Fig. 2 | Chemical gas sensing performance. a–**f**, Average response of a chip to NO_2 5 ppm (**a**), NH_3 50 ppm (**b**), H_2S 5 ppm (**c**), ethanol 200 ppm (**d**), acetone 200 ppm (**e**) and H_2 200 ppm (**f**). Average responses for each variation were obtained using 1,024 cMOF-CNFETs. After stabilization in dry air, the response of each chip to target gases was measured over 20 min, followed by recovery in dry air. The vertical dashed line at $t = 0$ min indicates the time when the device is exposed to the target gas, and the line at $t = 20$ min indicates the time when the device is exposed to dry air for recovery. The response is calculated as $I_D(t)/I_D(0)-1$ for NO_2 and $I_D(0)/I_D(t)-1$ for other target gases. **g**, *t*-SNE analysis. The response and threshold voltage change data were used to classify target gases. **h**, Comparison of the response with that of resistive-type devices. Bars represent the mean response for each material–gas pair, with black error bars indicating the standard deviation (s.d.). Individual data points are overlaid as dots. The horizontal spread of the dots reflects the local data density along the response axis, such that regions with a higher density appear visually thicker, providing a distribution-aware visualization of the response variability. The sample size is 1,024 for transistor-type sensors and 4 for resistive-type sensors.

As a first step, we functionalize the CNFET chip by growing four different cMOFs with the M_3L_2 structure[12,14] (where M = Ni or Co, and L = HHTP (2,3,6,7,10,11-hexahydroxytriphenylene) or HITP (2,3,6,7,10,11-hexaiminotriphenylene)) on the chip using a layer-by-layer (LBL) approach. In the second step, we further functionalize half (16 subarrays) of the cMOF-grown CNFETs (cMOF-CNFETs) by using 4 distinct metal ion solutions at 4 different concentrations and a reducing agent. This second functionalization is achieved by drop casting each solution onto the target subarrays using automatic microdispenser (M2 automation; Supplementary Fig. 1). To prevent droplet overflow between subarrays, we form microfluidic boundaries through a single photolithography process, followed by the deposition of a SAM before dispensing the solutions (Fig. 1i,j and Supplementary Fig. 2).

Figure 1c shows the optical microscopy (OM) image of a CNFET chip, and Fig. 1d–g shows scanning electron microscopy (SEM) images of a subarray containing 64 CNFETs, a CNFET with interdigitated electrodes, channel and drain electrodes of a CNFET after cMOF growth, and cMOF-CNT composites, respectively. Transmission electron microscopy (TEM) (Fig. 1h) confirms cMOF growth on CNT. Additional TEM images of cMOF-CNT composites after metal nanoparticle synthesis are provided in Supplementary Fig. 3. Figure 1k shows the average transfer characteristics of all Ni_3HHTP_2-grown CNFETs (NiHHTP-CNFETs) on a chip. The consistency of the chip functionalization methods is confirmed by the histograms of threshold voltage after cMOF growth (Fig. 1l). See Supplementary Note 1 and Supplementary Fig. 4 for the consistency of the CNFET chips before cMOF growth.

https://doi.org/10.1038/s44460-026-00037-z

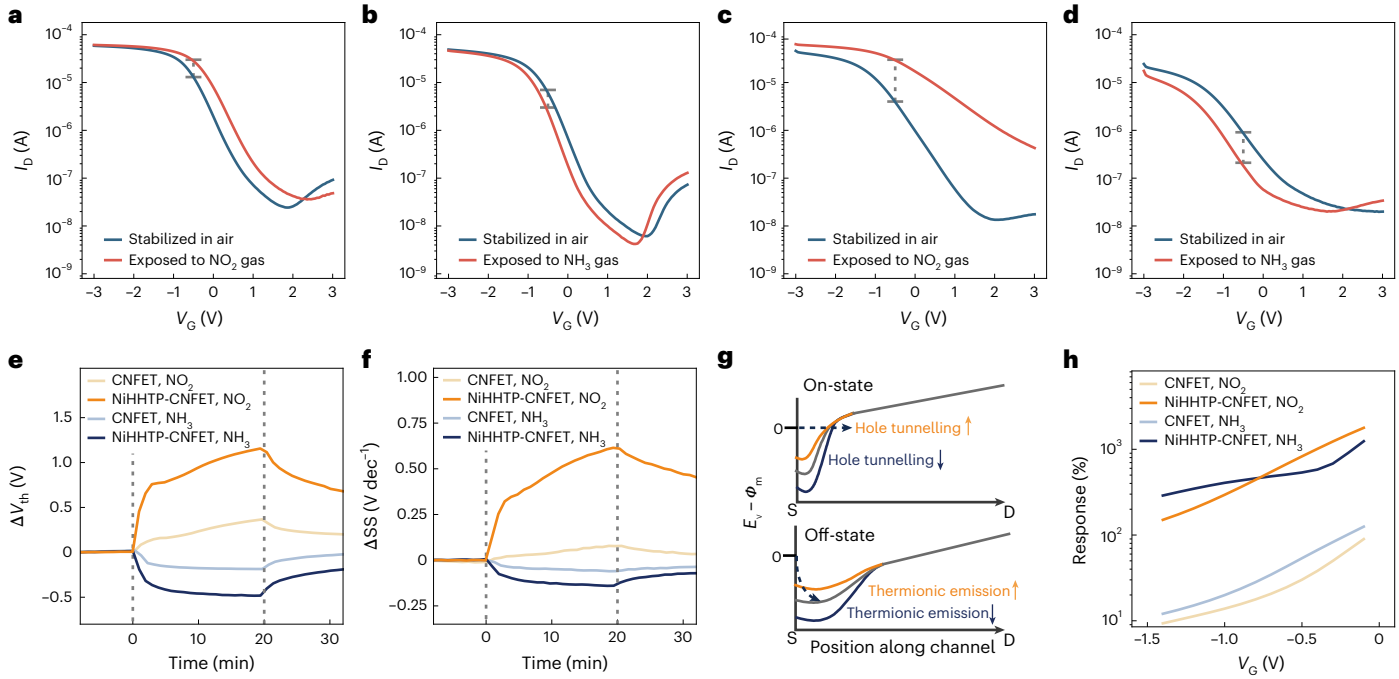

Fig. 3 | Analysis of device characteristics. a,**b**, Transfer characteristics change of CNFET upon NO_2 exposure (**a**) and NH_3 exposure (**b**). **c**,**d**, Transfer characteristics change of CNFET upon NO_2 exposure (**c**) and NH_3 (**d**). The modulation of transfer characteristics upon gas exposure is enhanced compared with unfunctionalized CNFETs. The dashed grey line in each plot is provided to compare the modulations in each corresponding case at $V_G = -0.5$ V. **e**,**f**, Threshold voltage change (**e**) and subthreshold swing (SS) change (**f**) of both CNFET and NiHHTP-CNFET upon NO_2 and NH_3 exposure. **g**, Illustration of Schottky barrier modulation in NiHHTP-CNFETs upon gas exposure near the source contact in the on-state (upper) and the off-state (lower). The *y* axis represents the relative potential, defined as the energy difference between the valence band edge (E_v) and the metal work function (Φ_m). The grey, orange and blue lines represent NiHHTP-CNFETs exposed to dry air, NO_2 and NH_3, respectively. In the on-state, upon NO_2 exposure, the reduction in the Schottky barrier for holes enhances the tunnelling current, whereas NH_3 exposure increases the Schottky barrier, decreasing the tunnelling current. In the off-state, modulation of the Schottky barrier affects thermionic emission, resulting in either an increase or decrease in leakage current and, consequently, a corresponding change in the subthreshold swing. **h**, Response of both NiHHTP-CNFET and CNFET to NO_2 and NH_3 gases with respect to the applied gate voltage.

As a control, we prepare resistive-type cMOF-CNT composite sensors and compare their performance with that of the cMOF-CNFET chips (see Supplementary Note 2 for details). The resistive-type cMOF-CNT sensors are also used to optimize the cMOF functionalization techniques on CNTs (Supplementary Note 2 and Supplementary Figs. 5 and 6). Although we mainly use NiHHTP in this work, the broad tunability of cMOF functionalization highlights the potential of other cMOF-CNT composites (Supplementary Note 3 and Supplementary Fig. 7) for gas sensing applications.

Effect of cMOF growth on gas sensing performance and analysis

Figure 2a–f shows the average response of 1,024 cMOF-CNFETs in 16 subarrays to 6 different gases: NO_2, NH_3, H_2S, ethanol, acetone and H_2 gas, at a gate voltage of −0.5 V ($V_G = -0.5$ V) and a source–drain voltage of 1 V ($V_{SD} = 1$ V) after stabilization in dry air (see Supplementary Figs. 8 and 9 for the gas flow system and gas measurement set-ups). To study the sensing mechanism, we focus particularly on the response of chips to 5 ppm NO_2 and 50 ppm NH_3. The concentrations of H_2S, ethanol, acetone and H_2 are chosen to be 5 ppm, 200 ppm, 200 ppm and 200 ppm, respectively, to achieve the similar magnitudes of response to each gas, thereby allowing us to assess the selectivity of our cMOF-CNT composites. See Supplementary Fig. 10 for a characterization at lower concentrations of target gases (0.5 ppm, 5 ppm, 0.5 ppm, 10 ppm, 10 ppm and 10 ppm for NO_2, NH_3, H_2S, ethanol, acetone and H_2 gas, respectively) and Supplementary Fig. 11 for repeatability across consecutive response–recovery cycles in dry air and at various humidity levels. The average response is calculated after excluding transistors damaged by the functionalization process, with an average exclusion rate of 3.6% per chip (Supplementary Note 4 and Supplementary Fig. 12). In addition, we correct background drift attributed to traps activated under continuous bias with the gate oxide in dry air[15,16] (Supplementary Note 4 and Supplementary Fig. 13). The response of cMOF-CNFETs to the six gases—NO_2, NH_3, H_2S, ethanol, acetone and H_2—increases by up to 108, 6.94, 139, 4.53, 3.51 and 5.56 times, respectively, compared with CNFETs before MOF growth at the same gate voltage.

We use *t*-distributed stochastic neighbour embedding (*t*-SNE) to visualize the separation among six gases based on average sensitivity and threshold-voltage shift dataset obtained from four different cMOF-CNFETs, each comprising 16 subarrays. For robustness beyond *t*-SNE, we use kernel principal component analysis to obtain deterministic embeddings showing class separability among the six gases, and we train a linear discriminant analysis classifier to evaluate classification performance (Supplementary Note 5 and Supplementary Figs. 14 and 15). Successful classification indicates the outstanding selectivity of the cMOF-CNT composite. Figure 2h compares the response of selected devices. We observe a 6.94-fold increase in response to NH_3 after NiHHTP is grown on CNFETs. Compared with unfunctionalized resistive-type CNT sensors, unfunctionalized CNFET chips exhibit a further 7.10-fold higher response, which we attribute to transconductance-driven amplification via optimal gate-voltage tuning (Supplementary Fig. 16). This confirms the importance of both material functionalization and device structure.

To explain the substantial improvement in the response of cMOF-CNFETs relative to CNT resistive sensors, we perform Raman scattering and analyse the transfer characteristics in the presence of representative electron-withdrawing and electron-donating gases, NO_2 and NH_3, respectively (Fig. 3a–d). Electronic transport in single-tube CNFETs is

https://doi.org/10.1038/s44460-026-00037-z

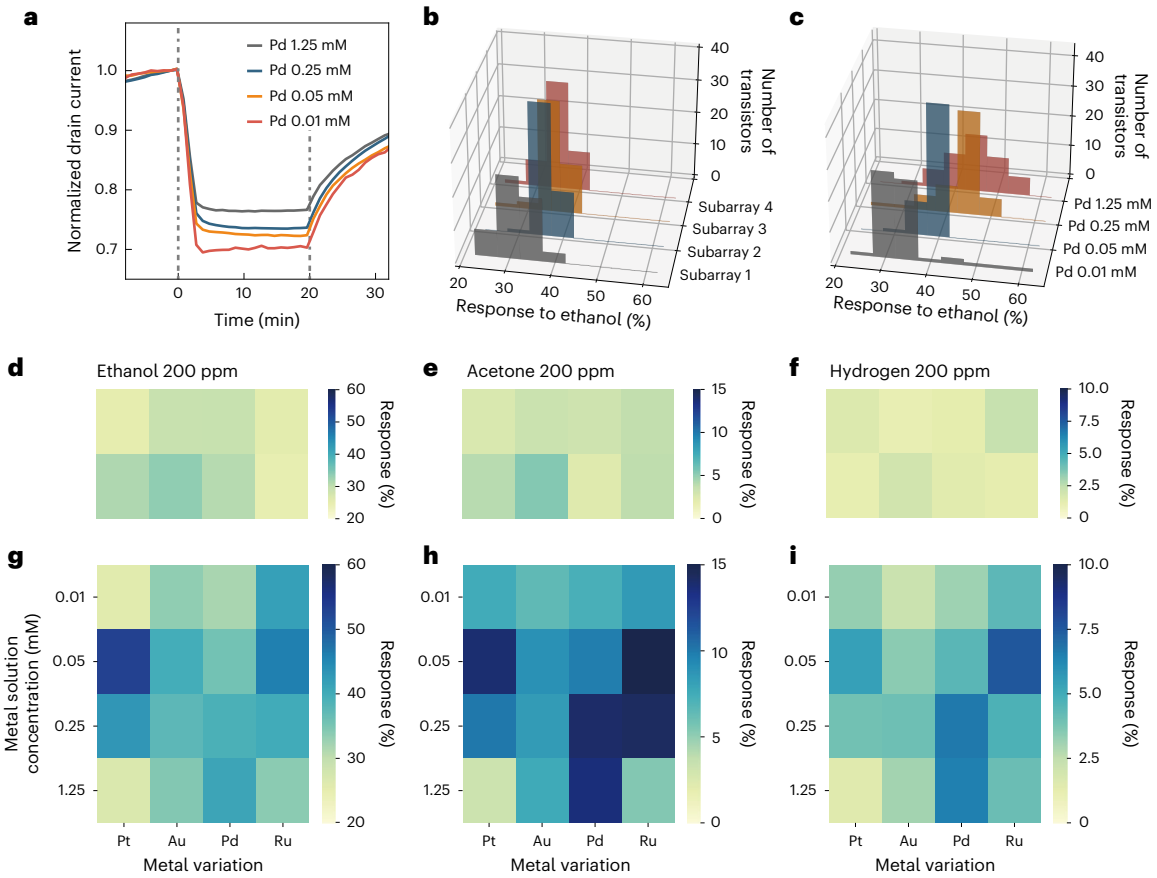

Fig. 4 | Metal nanoparticle synthesis. a, Average normalized drain current of 64 NiHHTP-CNFETs with Pd nanoparticle synthesized at four different concentrations. The functionalized CNFETs were stabilized under dry air at a flow rate of 1,000 sccm until $t = 0$ (min). The devices were then exposed to 200 ppm ethanol gas with a dry air balance for 20 min and were recovered under dry air from $t = 20$ (min). **b**,**c**, Histograms of the responses of four different subarrays to 200 ppm ethanol gas, with each subarray containing 64 NiHHTP-CNFETs: without metal nanoparticles (**b**) and with Pd nanoparticles synthesized at four different concentrations (**c**). **d**–**f**, Heatmap of average response of eight different NiHHTP-CNFETs subarrays to 200 ppm ethanol (**d**), acetone (**e**) and hydrogen gas (**f**). **g**–**i**, Heatmap of average response of NiHHTP-CNFETs functionalized with four distinct metals at four different concentrations to 200 ppm ethanol (**g**), acetone (**h**) and hydrogen gas (**i**).

understood to be controlled by a Schottky barrier at the source contact[17–19]. Four main factors can influence the drain current of CNFETs upon gas exposure: Schottky barrier height[20,21], CNT–CNT intertube junction barrier[22], intra-CNT doping[23] and disorder in the electronic states of the CNT[5]. For single-tube CNFET devices, previous studies have demonstrated that the operational mechanism of gas sensors is predominantly Schottky barrier modulation at the source contact[20,21]. In network CNFET devices, the role of intertube junction must also be considered, depending on the CNT network density[22]. Upon gas exposure, the intertube junction barrier and intertube charge hopping rate can be modulated by changes in local doping[24,25] or intercalation of gas molecules[26], causing changes in the saturation conductance[22].

As shown in Supplementary Fig. 17, the ex situ Raman studies are consistent with no doping effect in the unfunctionalized CNT channel and negligible changes in disorder in the electronic states of the CNT upon gas exposure (Supplementary Fig. 17a,b). Furthermore, the saturation conductance changes by 3.8% and 5.1% after 20 min of exposure to NO_2 and NH_3, respectively, implying a relatively small contribution from the intertube barrier modulation. Thus, in the absence of cMOF functionalization, the gas-induced shifts in threshold voltage and subthreshold swing (Fig. 3e,f) can be attributed to changes in the Schottky barrier height at the metal–CNT contacts[5].

By contrast, the Raman G-band peak of NiHHTP-CNFETs exhibits a blue shift upon exposure to NO_2, indicating p-type doping, and a red shift upon exposure to NH_3, indicating n-type doping[27] (Supplementary Fig. 17c,d). Because there is no doping effect in the unfunctionalized CNTs upon gas exposure, shifts in the G-band peak can be attributed to charge generated by the interaction between the cMOF layers and the gas (see Supplementary Note 6 for details). Charge transfer to CNT networks mediated by cMOF layers also substantially changes the saturation conductance by 27.4% and 32.9% upon 20 min of exposure to NO_2 and NH_3, respectively. Notably, the increase in the I_D/I_G ratio of NiHHTP-CNFETs after NO_2 exposure (Supplementary Fig. 17d) indicates the generation of additional defect states, which could explain the much larger change in subthreshold swing compared with NH_3, resulting in a pronounced response in the subthreshold regime (Fig. 3h). In summary, in addition to the Schottky barrier height change at the metal–CNT contact, cMOF functionalization maximizes the sensor response via charge transfer from cMOF, thereby modulating both intertube junctions and intratube doping.

Integration of CNFET-based sensor array

In addition to enhancing the sensitivity and selectivity towards the target gas, integrating multiple sensors with distinct responses onto a single chip presents a major challenge. To address this issue, we introduce the second functionalization step, involving the in situ synthesis of 4 distinct metal nanoparticles at 4 different concentrations across 16 selected subarrays out of a total of 32 (Methods). The remaining 16 subarrays are used to validate the statistical significance of the modulation introduced by the metal nanoparticles.

https://doi.org/10.1038/s44460-026-00037-z

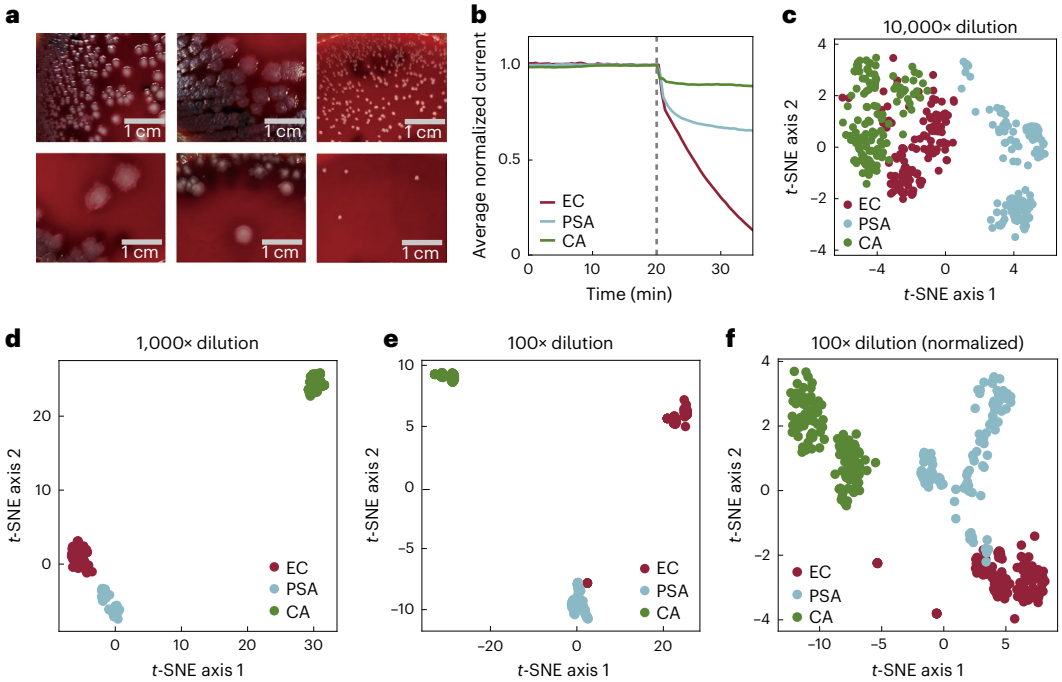

Fig. 5 | Medical application: biological gas sensing. a, Images of EC, PSA and CA, grown on agar plate, from left to right. The initial concentrations are 100-fold dilution (top), and 1,000-fold dilution (bottom) of 0.5 McF broth. **b**, Transient response of chips to 100-fold diluted EC, PSA and CA. The chip was stabilized with agar plate without bacteria or yeast until 20 min, and then exposed to the target bacteria or yeast. **c**–**e**, *t*-SNE analysis of 10,000-fold (**c**), 1,000-fold (**d**) and 100-fold dilution (**e**) of 0.5 McF from the raw dataset. **f**, *t*-SNE analysis of 100-fold dilution of 0.5 McF using only the normalized dataset.

After metal nanoparticle synthesis, the response of NiHHTP-CNFETs to ethanol increases as the concentration of the Pd solution increases (Fig. 4a). To demonstrate that improvements in selectivity are due to metal nanoparticles and not an artefact of device-to-device variation, we compare histograms of four different NiHHTP-CNFET subarrays without and with metal nanoparticles (Fig. 4b,c). For the former histograms, which represent subarrays without metal nanoparticles, the mean values of the responses across 64 functionalized transistors in each subarray are 30.2%, 33.5%, 33.9% and 32.6%, with low standard deviations of 3.2%, 2.2%, 2.6% and 3.0%, respectively. By contrast, the histogram for subarrays with metal nanoparticles shifts as the concentration increases, showing the increasing mean response values of 31.8%, 35.7%, 40.0% and 41.2%, accompanied by low standard deviation of 6.9%, 1.8%, 5.9% and 6.3%, respectively.

Figure 4d–f shows heatmaps of the average responses of 64 NiHHTP-CNFETs from 8 different subarrays to 3 different target gases: ethanol, acetone and hydrogen, respectively. We intentionally adjust the heat map scale bar for each gas to compare the degree of modulation between responses without metal nanoparticles and those with metal nanoparticles. We confirm that the average responses from 8 NiHHTP-CNFETs subarrays are consistent, whereas the 16 subarrays with metal nanoparticles exhibit distinct patterns for each gas (Fig. 4g–i). This distinct pattern allows the classification of gases using an integrated chip, while the low subarray-to-subarray variation and device-to-device variation in each subarray statistically supports the generated response pattern. With a uniform scale bar, response patterns are more distinct, enabling easier classification (Supplementary Fig. 18). See Supplementary Fig. 19 for reversible characteristics of NiHHTP-CNFETs.

In particular, among the four NiHHTP-CNT composites loaded with different metal nanoparticles, the 1.25 mM Pd-loaded sample exhibits the highest responses to ethanol and acetone. This is consistent with the red shifts observed in the Raman G-band spectrum (Supplementary Fig. 20), indicating that metal nanoparticles promote interfacial charge transfer and induce corresponding doping effects on the CNT channel. High-resolution TEM further reveals that higher precursor concentrations (1.25 and 0.25 mM) produce both ultrasmall (<2 nm) catalysts confined within the cMOF pores and some agglomerated nanoparticles, whereas lower concentrations (0.05 and 0.01 mM) mainly yield confined catalysts (Supplementary Fig. 21). This indicates that excessive catalyst loading leads to surface coverage of the cMOF matrix and may block intrinsic active sites[28]. Consequently, the response enhancement is expected to exhibit a peak for a particular loading of metal nanoparticles, consistent with our observations (Fig. 4g–i). This statistically supported nonlinear dependence reduces feature collinearity and increases a class separability[29], indicating that not only the catalyst type but also the size and density play critical roles in sensor performance.

Medical application

One of the most important qualities of an integrated gas sensing chip is its potential to address real-time challenges related to human or biological problems. However, most previous chemical sensing studies have relied on high temperature operation[3,30,31] or bulky, non-portable systems[32], limiting their use in real-world biomedical applications (Supplementary Note 7 and Supplementary Fig. 22). We present a simple method for classifying bacteria and yeast on the basis of gases generated during growth, using our functionalized CNFET array with a portable measurement circuit placed over the culture plate (Supplementary Fig. 23). We compare responses to the common intestinal bacterium EC, a bacterial pathogen, PSA and a pathogenic yeast, CA. Each is prepared from broth at a 0.5 McFarland standard (McF), then diluted to 1/100, 1/1,000 and 1/10,000-fold and finally incubated on agar plates for 24 h (Supplementary Note 8). Figure 5a shows the images of EC, PSA and CA (from left to right) with the concentrations of 1/100 (top) and 1/1,000 (bottom). See Supplementary Note 9 for major volatile organic compounds emitted by the three microorganisms. We first stabilize the chip by putting the chip and a bacteria-free agar plate in a small container (Supplementary Note 10). Subsequently, we replace these plates with incubated plates and record the electrical response as a function of exposure time.

The responses of NiHHTP-CNFETs to the gases emitted from plates incubated with 1/100 dilutions are clear (Fig. 5b). Control experiments with agar plates inserted after the stabilization step confirm that the response to biological gases are not false signals (Supplementary Fig. 24). In addition, we verify the consistency of our chip in terms of device-to-device and chip-to-chip variations by comparing response averages and histograms (Supplementary Fig. 25). Conventional *t*-SNE readily distinguishes the 1/100 and 1/1,000 dilution samples, with lower separation for 1/10,000 dilution samples (Fig. 5c–e). Furthermore, we demonstrate a 3-week stability test in which new cultures of each microorganism were grown weekly and tested by the same chips (Supplementary Fig. 26). Despite the stochastic nature of microbial growth, we achieve 95.0% classification accuracy in identifying microorganisms, confirming the robustness of our gas sensing system.

To further evaluate the selectivity of our NiHHTP-CNFETs with metal nanoparticles, we normalize the responses of the 1/100 dilution samples (see Supplementary Note 11 for details), thereby removing any information contained in the magnitude of the signals. Classification of bacteria is still achieved using the normalized dataset (Fig. 5f), suggesting that the successful classification is attributable not only to the magnitudes of the response of NiHHTP-CNFETs, but also to the selectivity introduced by metal nanoparticle functionalization. To examine whether different concentrations of the same microorganisms can be classified as the same class based on the selectivity, we demonstrate concentration-invariant pathogen classification using a linear discriminant analysis classifier. When training and testing on two concentrations (1/100 and 1/1,000-fold dilutions) and three concentrations (1/100, 1/1,000 and 1/10,000-fold dilutions), the classification accuracies are 99.6% and 95.5% (Supplementary Fig. 27), respectively, indicating that reliable pathogen identification can be maintained despite changes in concentration.

Conclusion

We demonstrate room-temperature gas sensing using foundry-derived, integrated CNFET chips. By contrast, previous proof-of-concept studies have combined data from sensors fabricated on different substrates. Because many chemical and biological materials are incompatible with traditional lithography, the CNFET chips are functionalized with cMOFs using a low-cost LBL coating process. The LBL method enables precise control of cMOF thickness and composition and allows the confinement of ultrasmall catalytic metal nanoparticles within cMOF pores. Functionalization increases the sensitivity by up to two orders of magnitude, with patterned synthesis of catalytic metal nanoparticles enabling discrimination between different analytes on a single chip.

To enable portable microelectronic chemical sensors for general biomedical applications, the sensors should ideally operate at room temperature. High-temperature operation often requires a gas-flow system with a non-portable carrier-gas cylinder or a complex pump module to prevent heating of samples or exposure to human participants. At the same time, the sensors must be sufficiently sensitive to detect trace levels of volatile organic compounds at room temperature. In addition, to obtain statistically significant datasets, the sensing platform should exhibit minimal device-to-device variation and be readily integrated. We demonstrate label-free, diffusion-limited classification of bacteria and yeast by analysing the gases they emit in real-world settings, without the need for a carrier-gas cylinder or any other complex module that may be incompatible with on-chip integration. The resulting combination of performance and scalable manufacturing promises to introduce the traditional advantages of microelectronics to applications in chemical gas sensing.

Methods

CNFET fabrication

CNFETs chips were fabricated on 200-mm silicon wafers by SkyWater Technology[13]. As a first step, the 200-mm silicon wafer was planarized and metal gates were defined through a tungsten plug damascene process. Next, HfO_2 was deposited by atomic layer deposition. For the CNT layer, CNTs dispersed in toluene at a 1:20 ratio were poured into a polytetrafluoroethylene container holding the wafer and incubated for 48 h to achieve uniform coverage. The CNT solution comprises ≥99.99% semiconducting single-walled CNTs dispersed in toluene. The CNTs were synthesized by a radiofrequency plasma method, and the CNT solution was prepared via a customized process derived from NanoIntegris' IsoSol-S100 polymer-wrapped single-walled CNT solution (see https://nanointegris.com for more information about polymer-wrapped nanotubes). Semiconducting enrichment was achieved by exploiting the selective affinity of conjugated polymers for semiconducting CNTs[33,34]. The deposited CNT density is ~75 CNTs μm^{-1}, with an average length of 1.6 µm and average diameter of 1.2 nm. Following incubation, the wafer was rinsed sequentially with acetone and isopropyl alcohol to remove excess CNTs. Finally, for the source and drain contacts, a Ti/Pt layer was deposited and patterned using the e-beam evaporation and lift-off process. The distance between the source electrode and drain electrode is 3 µm. Oxygen plasma etching was used to remove CNTs outside the active region of the chip. See previous works for additional details of the fabrication process[13,35,36].

Material preparation

For cMOF growth, NaOAc (Alfa Aesar), cobalt(II) nitrate hexahydrate ($Co(NO_3)_2{\cdot}6H_2O$) (Alfa Aesar), copper(II) sulfate pentahydrate ($Cu(SO_4){\cdot}5H_2O$) (Alfa Aesar), nickel(II) acetate tetrahydrate ($Ni(OAc)_2{\cdot}4H_2O$) (Strem) precursors and HHTP (TCI Chemicals) were used without further purification. 2,3,6,7,10,11-Hexaiminotriphenylene hexahydrochloride (HATP·6HCl) was synthesized according to procedures reported previously[1]. For metal nanoparticle synthesis, potassium tetrachloroplatinuate(II) (K_2PtCl_4), potassium tetrachloropalladate(II) (Cl_4K_2Pd), potassium gold(III) chloride ($KAuCl_4$), potassium hexachlororuthenate(IV) (K_2RuCl_6) and sodium borohydride ($NaBH_4$), trichloro(1*H*,1*H*,2*H*,2*H*-perfluorooctyl)silane were purchased from Sigma-Aldrich. Acetone, isopropyl alcohol and ethanol were used as received without further purification.

cMOF growth

The target metal precursor and ligand were dissolved in ethanol, with concentrations of 0.1 mM and 0.01 mM, respectively. The first step in the cMOF growth process is to activate the surface of the CNFETs using an ultraviolet ozone cleaner for 3 min at a power of 10 mW to introduce hydroxyl groups[37]. This ultraviolet ozone cleaning process facilitates the self-assembly of positively charged metal ions on the negatively charged hydroxyl groups. Subsequently, a LBL growth process was conducted by repeatedly dipping the substrate into the metal precursor solution and the organic ligand solution, with washing in ethanol between each step. The number of LBL cycles was controlled from 1 to 30 cycles for the resistive-type devices and set to 6 cycles for the CNFET chips. Following the LBL process, the CNFETs chips were annealed at 65 °C for 30 min.

Microfluidic boundary formation

The microfluidic boundaries were formed through a photolithography process and the deposition of a SAM. Initially, a positive photoresist was spin-coated onto the CNFET chip. Through photolithography, the photoresist was removed from the chip's surface, except for the active region where the 32 subarrays of CNFETs are located. Subsequently, the chip, along with trichloro(1*H*,1*H*,2*H*,2*H*-perfluorooctyl)silane, was placed in a vacuum chamber for 2 h to deposit SAM layers and make the surface superhydrophobic. Finally, the remaining photoresist on the active region and any excess SAM layers were removed by cleaning the chip with acetone and isopropyl alcohol.

Metal nanoparticle synthesis

The metal precursors (Pt, Au, Pd and Ru) were dissolved in water at concentrations of 0.01 mM, 0.05 mM, 0.25 mM and 1.25 mM for each

metal, resulting in a total of 16 different metal solutions. Sodium borohydride, used as the reducing agent, was also dissolved in water at a concentration of 0.1 mM. These 16 metal solutions were dispensed onto 16 subarrays using an automated microdispenser (M2 Automation) at 2-min intervals, with 5 droplets drop cast on each subarray. Subsequently, the ligand solution was dispensed using the same procedure. The chip was then rinsed with water and annealed at 65 °C.

Chemical gas sensing

The target gases, including NO_2, NH_3, H_2S, ethanol, acetone and hydrogen, were purchased from Airgas, with their initial concentrations in dry air being 50 ppm, 1,000 ppm, 50 ppm, 200 ppm, 200 ppm and 200 ppm, respectively. NO_2, NH_3 and H_2S were diluted using mass flow controllers and an additional dry air gas cylinder to concentrations of 5 ppm, 50 ppm and 5 ppm, respectively, while ethanol, acetone and hydrogen were used without further dilution. The target gas was introduced at a flow rate of 1,000 sccm to the gas inlet of a custom-built circuit to expose the CNFET chip to the gas. The chips were first exposed to dry air for 70 min to be stabilized, followed by exposure to the target gas for 20 min. During gas exposure, a single transfer curve was measured every minute for each of the 2,048 CNFETs on the chip, with a gate voltage range of −3 V to 3 V (from −3 V to 3 V) and a source–drain voltage of 1 V. It takes 5 s to measure all 2,048 CNFETs.

Biological sample preparation

EC, PSA and CA were purchased from ATCC, with strain numbers of 25922, 27853 and 18804, respectively. See Supplementary Note 5 for details.

Material characterization

Raman analysis was measured using a Renishaw Invia Reflex Raman Confocal Microscope with a 532-nm laser. SEM characterization was performed at MIT.nano using a Gemini 450 SEM (Zeiss). TEM characterization was performed at MIT.nano using an FEI Tecnai 120 kV electron microscope. X-ray photoelectron spectroscopy characterization was performed at MIT.nano using a Physical Electronics PHI Versaprobe II XPS equipped with an Al anode as the X-ray source. The charge shift was calibrated by setting the C1*s* peak of surface-adsorbed adventitious carbon to 284.8 eV.

Reporting summary

Further information on research design is available in the Nature Portfolio Reporting Summary linked to this article.

Data availability

The datasets collected for various gases and microorganisms in this study are available via GitHub at https://github.com/Jaekang-Song/cMOF_CNFETs_Gas_Sensor. Further data supporting the other findings of this study are available from the corresponding author upon request.

Code availability

The code used in this study is available via GitHub at https://github.com/Jaekang-Song/cMOF_CNFETs_Gas_Sensor.

References

1. Campbell, M. G., Liu, S. F., Swager, T. M. & Dincă, M. Chemiresistive sensor arrays from conductive 2D metal–organic frameworks. *J. Am. Chem. Soc.* **137**, 13780–13783 (2015).
2. Chen, J. et al. Ultra-low-power smart electronic nose system based on three-dimensional tin oxide nanotube arrays. *ACS Nano* **12**, 6079–6088 (2018).
3. Wang, C. et al. Biomimetic olfactory chips based on large-scale monolithically integrated nanotube sensor arrays. *Nat. Electron.* **7**, 157–167 (2024).
4. Kang, H. et al. Multiarray nanopattern electronic nose (E-Nose) by high-resolution top-down nanolithography. *Adv. Funct. Mater.* **30**, 2002486 (2020).
5. Schroeder, V., Savagatrup, S., He, M., Lin, S. & Swager, T. M. Carbon nanotube chemical sensors. *Chem. Rev.* **119**, 599–663 (2019).
6. Cho, T. S., Lee, K.-J., Kong, J. & Chandrakasan, A. P. A Low power carbon nanotube chemical sensor system. In *2007 IEEE Custom Integrated Circuits Conference* 181–184 (IEEE, 2007); https://doi.org/10.1109/CICC.2007.4405708
7. Freddi, S. et al. Development of a sensing array for human breath analysis based on SWCNT layers functionalized with semiconductor organic molecules. *Adv. Healthc. Mater.* **9**, 2000377 (2020).
8. Star, A., Joshi, V., Skarupo, S., Thomas, D. & Gabriel, J.-C. P. Gas sensor array based on metal-decorated carbon nanotubes. *J. Phys. Chem. B* **110**, 21014–21020 (2006).
9. Fennell, J. F., Hamaguchi, H., Yoon, B. & Swager, T. M. Chemiresistor devices for chemical warfare agent detection based on polymer wrapped single-walled carbon nanotubes. *Sensors* **17**, 982 (2017).
10. Wang, F. & Swager, T. M. Diverse chemiresistors based upon covalently modified multiwalled carbon nanotubes. *J. Am. Chem. Soc.* **133**, 11181–11193 (2011).
11. Zeng, Z. et al. Heterogeneous growth of UiO-66-NH_2 on oxidized single-walled carbon nanotubes to form "beads-on-a-string" composites. *ACS Appl. Mater. Interfaces* **13**, 15482–15489 (2021).
12. Ha, D.-G. et al. Large single crystals of two-dimensional π-conjugated metal–organic frameworks via biphasic solution-solid growth. *ACS Cent. Sci.* **7**, 104–109 (2021).
13. Bishop, M. D. et al. Fabrication of carbon nanotube field-effect transistors in commercial silicon manufacturing facilities. *Nat. Electron.* **3**, 492–501 (2020).
14. Chen, T. et al. Continuous electrical conductivity variation in M3(Hexaiminotriphenylene)2 (M = Co, Ni, Cu) MOF alloys. *J. Am. Chem. Soc.* **142**, 12367–12373 (2020).
15. Libsch, F. R. & Kanicki, J. Bias-stress-induced stretched-exponential time dependence of charge injection and trapping in amorphous thin-film transistors. *Appl. Phys. Lett.* **62**, 1286–1288 (1993).
16. Lee, S. W. et al. Positive gate bias stress instability of carbon nanotube thin film transistors. *Appl. Phys. Lett.* **101**, 053504 (2012).
17. Appenzeller, J. et al. Field-modulated carrier transport in carbon nanotube transistors. *Phys. Rev. Lett.* **89**, 126801 (2002).
18. Zhang, J., Wang, C., Fu, Y., Che, Y. & Zhou, C. Air-stable conversion of separated carbon nanotube thin-film transistors from p-type to n-type using atomic layer deposition of high-κ oxide and its application in CMOS logic circuits. *ACS Nano* **5**, 3284–3292 (2011).
19. Lau, C., Srimani, T., Bishop, M. D., Hills, G. & Shulaker, M. M. Tunable n-type doping of carbon nanotubes through engineered atomic layer deposition HfO_x films. *ACS Nano* **12**, 10924–10931 (2018).
20. Peng, N., Zhang, Q., Chow, C. L., Tan, O. K. & Marzari, N. Sensing mechanisms for carbon nanotube based NH_3 gas detection. *Nano Lett.* **9**, 1626–1630 (2009).
21. Zhang, J., Boyd, A., Tselev, A., Paranjape, M. & Barbara, P. Mechanism of NO_2 detection in carbon nanotube field effect transistor chemical sensors. *Appl. Phys. Lett.* **88**, 123112 (2006).
22. Boyd, A., Dube, I., Fedorov, G., Paranjape, M. & Barbara, P. Gas sensing mechanism of carbon nanotubes: from single tubes to high-density networks. *Carbon* **69**, 417–423 (2014).
23. Salehi-Khojin, A. et al. On the sensing mechanism in carbon nanotube chemiresistors. *ACS Nano* **5**, 153–158 (2011).

24. Léonard, F. & Tersoff, J. Novel length scales in nanotube devices. *Phys. Rev. Lett.* **83**, 5174–5177 (1999).
25. Léonard, F. & Tersoff, J. Role of Fermi-level pinning in nanotube Schottky diodes. *Phys. Rev. Lett.* **84**, 4693–4696 (2000).
26. Mowbray, D. J., Morgan, C. & Thygesen, K. S. Influence of O_2 and N_2 on the conductivity of carbon nanotube networks. *Phys. Rev. B* **79**, 195431 (2009).
27. Voggu, R., Rout, C. S., Franklin, A. D., Fisher, T. S. & Rao, C. N. R. Extraordinary sensitivity of the electronic structure and properties of single-walled carbon nanotubes to molecular charge-transfer. *J. Phys. Chem. C* **112**, 13053–13056 (2008).
28. Hwang, I.-S. et al. Facile control of C_2H_5OH sensing characteristics by decorating discrete Ag nanoclusters on SnO_2 nanowire networks. *ACS Appl. Mater. Interfaces* **3**, 3140–3145 (2011).
29. Peng, H., Long, F. & Ding, C. Feature selection based on mutual information criteria of max-dependency, max-relevance, and min-redundancy. *IEEE Trans. Pattern Anal. Mach. Intell.* **27**, 1226–1238 (2005).
30. Sun, H. et al. Sensor array optimization of electronic nose for detection of bacteria in wound infection. *IEEE Trans. Ind. Electron.* **64**, 7350–7358 (2017).
31. Seesaard, T., Thippakorn, C., Kerdcharoen, T. & Kladsomboon, S. A hybrid electronic nose system for discrimination of pathogenic bacterial volatile compounds. *Anal. Methods* **12**, 5671–5683 (2020).
32. Chen, J. et al. Characterization of the key aroma compounds in different yeast proteins by GC–MS/O, sensory evaluation, and E-Nose. *Foods* **12**, 3136 (2023).
33. Brady, G. J. et al. Polyfluorene-sorted, carbon nanotube array field-effect transistors with increased current density and high on/off ratio. *ACS Nano* **8**, 11614–11621 (2014).
34. Ding, J. et al. A hybrid enrichment process combining conjugated polymer extraction and silica gel adsorption for high purity semiconducting single-walled carbon nanotubes (SWCNT). *Nanoscale* **7**, 15741–15747 (2015).
35. Srimani, T. et al. Foundry monolithic 3D BEOL transistor + memory stack: iso-performance and iso-footprint BEOL carbon nanotube FET+RRAM vs. FEOL silicon FET+RRAM. In *2023 IEEE Symposium on VLSI Technology and Circuits* 1–2 (IEEE, 2023); https://doi.org/10.23919/VLSITechnologyandCir57934.2023.10185414
36. Yu, A. C. et al. Foundry integration of carbon nanotube FETs with 320 nm contacted gate pitch using new lift-off-free process. *IEEE Electron Device Lett.* **43**, 486–489 (2022).
37. Kumar, S. et al. Sensitive detection of a gaseous analyte with low-power metal–organic framework functionalized carbon nanotube transistors. *Adv. Electron. Mater.* **10**, 2300533 (2024).

Acknowledgements

This work was supported by Analog Devices Inc.

Author contributions

J.S., D.K., S.F., M. Shulaker, M.D. and M.B. conceived the project. J.S., D.K. and M.B. wrote the paper. Device fabrication, characterization and chemical gas sensing measurements were carried out by J.S. and D.K. under guidance of M. Shulaker, M.D. and M.B. J.T. helped with the fabrication process development. The gas testing set-up was built by J.S., D.K. and Y.-.M.J. G.M. and M. Song prepared bacteria and yeast. J.S. performed the biological gas sensing experiments, and G.M. assisted with the measurements under the guidance of M. Shulaker. Chemicals for cMOF growth and metal nanoparticle synthesis were prepared by D.K., Y.-M.J., T.C. and J.W. The device measurement set-up was built by A.C. and S.P. D.K. helped with device fabrication and gas sensing measurements. All authors discussed the results presented in this paper.

Competing interests

The authors declare no competing interests.

Additional information

Supplementary information The online version contains supplementary material available at https://doi.org/10.1038/s44460-026-00037-z.

Correspondence and requests for materials should be addressed to Max Shulaker, Mircea Dincă or Marc Baldo.

Peer review information *Nature Sensors* thanks Il-Doo Kim, Hiroshi Tabata and the other, anonymous, reviewer(s) for their contribution to the peer review of this work.

nature portfolio

Corresponding author(s): Marc A. Baldo

Last updated by author(s): Jan 12, 2026

Reporting Summary

Nature Portfolio wishes to improve the reproducibility of the work that we publish. This form provides structure for consistency and transparency in reporting. For further information on Nature Portfolio policies, see our Editorial Policies and the Editorial Policy Checklist.

Statistics

For all statistical analyses, confirm that the following items are present in the figure legend, table legend, main text, or Methods section.

n/a	Confirmed
☐	☒ The exact sample size (*n*) for each experimental group/condition, given as a discrete number and unit of measurement
☐	☒ A statement on whether measurements were taken from distinct samples or whether the same sample was measured repeatedly
☒	☐ The statistical test(s) used AND whether they are one- or two-sided *Only common tests should be described solely by name; describe more complex techniques in the Methods section.*
☒	☐ A description of all covariates tested
☐	☒ A description of any assumptions or corrections, such as tests of normality and adjustment for multiple comparisons
☐	☒ A full description of the statistical parameters including central tendency (e.g. means) or other basic estimates (e.g. regression coefficient) AND variation (e.g. standard deviation) or associated estimates of uncertainty (e.g. confidence intervals)
☒	☐ For null hypothesis testing, the test statistic (e.g. *F*, *t*, *r*) with confidence intervals, effect sizes, degrees of freedom and *P* value noted *Give P values as exact values whenever suitable.*
☒	☐ For Bayesian analysis, information on the choice of priors and Markov chain Monte Carlo settings
☒	☐ For hierarchical and complex designs, identification of the appropriate level for tests and full reporting of outcomes
☒	☐ Estimates of effect sizes (e.g. Cohen's *d*, Pearson's *r*), indicating how they were calculated

Our web collection on statistics for biologists contains articles on many of the points above.

Software and code

Policy information about availability of computer code

Data collection	No software was used for data collection. The data used in this study were obtained by directly measuring electrical signals.
Data analysis	Data analysis was performed using custom python code. Software is not central to this research. The code used in this study can be found in a publicly accessible repository (https://github.com/Jaekang-Song/cMOF_CNFETs_Gas_Sensor).

For manuscripts utilizing custom algorithms or software that are central to the research but not yet described in published literature, software must be made available to editors and reviewers. We strongly encourage code deposition in a community repository (e.g. GitHub). See the Nature Portfolio guidelines for submitting code & software for further information.

Data

Policy information about availability of data

All manuscripts must include a data availability statement. This statement should provide the following information, where applicable:

- Accession codes, unique identifiers, or web links for publicly available datasets
- A description of any restrictions on data availability
- For clinical datasets or third party data, please ensure that the statement adheres to our policy

The datasets collected for various gases and microorganisms in this study can be found in a publicly accessible repository (https://github.com/Jaekang-Song/cMOF_CNFETs_Gas_Sensor). Further data supporting the other findings of this study are available from the corresponding author upon request.

Research involving human participants, their data, or biological material

Policy information about studies with human participants or human data. See also policy information about sex, gender (identity/presentation), and sexual orientation and race, ethnicity and racism.

Reporting on sex and gender	*Use the terms sex (biological attribute) and gender (shaped by social and cultural circumstances) carefully in order to avoid confusing both terms. Indicate if findings apply to only one sex or gender; describe whether sex and gender were considered in study design; whether sex and/or gender was determined based on self-reporting or assigned and methods used. Provide in the source data disaggregated sex and gender data, where this information has been collected, and if consent has been obtained for sharing of individual-level data; provide overall numbers in this Reporting Summary. Please state if this information has not been collected. Report sex- and gender-based analyses where performed, justify reasons for lack of sex- and gender-based analysis.*
Reporting on race, ethnicity, or other socially relevant groupings	*Please specify the socially constructed or socially relevant categorization variable(s) used in your manuscript and explain why they were used. Please note that such variables should not be used as proxies for other socially constructed/relevant variables (for example, race or ethnicity should not be used as a proxy for socioeconomic status). Provide clear definitions of the relevant terms used, how they were provided (by the participants/respondents, the researchers, or third parties), and the method(s) used to classify people into the different categories (e.g. self-report, census or administrative data, social media data, etc.) Please provide details about how you controlled for confounding variables in your analyses.*
Population characteristics	*Describe the covariate-relevant population characteristics of the human research participants (e.g. age, genotypic information, past and current diagnosis and treatment categories). If you filled out the behavioural & social sciences study design questions and have nothing to add here, write "See above."*
Recruitment	*Describe how participants were recruited. Outline any potential self-selection bias or other biases that may be present and how these are likely to impact results.*
Ethics oversight	*Identify the organization(s) that approved the study protocol.*

Note that full information on the approval of the study protocol must also be provided in the manuscript.

Field-specific reporting

Please select the one below that is the best fit for your research. If you are not sure, read the appropriate sections before making your selection.

☐ Life sciences ☐ Behavioural & social sciences ☒ Ecological, evolutionary & environmental sciences

For a reference copy of the document with all sections, see nature.com/documents/nr-reporting-summary-flat.pdf

Ecological, evolutionary & environmental sciences study design

All studies must disclose on these points even when the disclosure is negative.

Study description	This study reports a multichannel gas-sensing platform based on arrays of carbon nanotube field-effect transistors (CNFETs) functionalized with conductive metal-organic frameworks and metal nanoparticles.
Research sample	We measured the low concentrations of various chemical gases: nitrogen dioxide, ammonia, hydrogen sulfide, ethanol, acetone, and hydrogen. We also measured biological samples consisting of agar-grown cultures of three clinically relevant microorganisms: Escherichia coli, Pseudomonas aeruginosa, and Candida albican.
Sampling strategy	Each CNFET within the array was treated as an independent sensing unit, as each CNFET can be individually addressable, providing large number of parallel measurements. Multiple chips and repeated exposures to each microorganisms were used to generate training and testing datasets. We have demonstrated a three-week stability test in which new cultures of each microorganism were grown weekly and tested by the multiple chips.
Data collection	Authors recorded the data using electrical reader which is fabricated at Analog Devices Incorporated. Electrical current-voltage characteristics of each CNFET were recorded. For chemical gas sensing, we used MFCs to flow gases. For biological gas sensing, microbial cultures were placed in a sealed measurement chamber to ensure diffusion-limited exposure.
Timing and spatial scale	Our chip size is 6 mm * 10 mm. In the three-week stability test mentioned above, we measured biological plates once a week to test the long-term stability of devices and variability in the biological samples.
Data exclusions	Individual CNFET showing device failure, open circuit, or short circuit values were excluded from analysis. We describe the pruning procedure in Main text and Supplementary Information.
Reproducibility	The experiments were repeated across multiple chips and multiple independently prepared microbial cultures. Consistent response patterns and classification performance using LDA were observed across repeats.

Randomization	Our sensor groups are deterministically defined by the chip architecture and functionalized layout, and chemical and biological samples are defined by species identity for classification.
Blinding	Blinding was not applicable because all sensor measurements were acquired automatically by electronic instrumentation and did not involve subjective human judgment.

Did the study involve field work? ☐ Yes ☒ No

Reporting for specific materials, systems and methods

We require information from authors about some types of materials, experimental systems and methods used in many studies. Here, indicate whether each material, system or method listed is relevant to your study. If you are not sure if a list item applies to your research, read the appropriate section before selecting a response.

Materials & experimental systems

n/a	Involved in the study
☒	☐ Antibodies
☒	☐ Eukaryotic cell lines
☒	☐ Palaeontology and archaeology
☒	☐ Animals and other organisms
☒	☐ Clinical data
☒	☐ Dual use research of concern
☒	☐ Plants

Methods

n/a	Involved in the study
☒	☐ ChIP-seq
☒	☐ Flow cytometry
☒	☐ MRI-based neuroimaging

Plants

Seed stocks	*Report on the source of all seed stocks or other plant material used. If applicable, state the seed stock centre and catalogue number. If plant specimens were collected from the field, describe the collection location, date and sampling procedures.*
Novel plant genotypes	*Describe the methods by which all novel plant genotypes were produced. This includes those generated by transgenic approaches, gene editing, chemical/radiation-based mutagenesis and hybridization. For transgenic lines, describe the transformation method, the number of independent lines analyzed and the generation upon which experiments were performed. For gene-edited lines, describe the editor used, the endogenous sequence targeted for editing, the targeting guide RNA sequence (if applicable) and how the editor was applied.*
Authentication	*Describe any authentication procedures for each seed stock used or novel genotype generated. Describe any experiments used to assess the effect of a mutation and, where applicable, how potential secondary effects (e.g. second site T-DNA insertions, mosiacism, off-target gene editing) were examined.*